http://doi.org/10.22364/ncmesc.02

2. Synthesis and research of electrode and solid electrolyte materials for lithium ion batteries

Litija jonu bateriju elektrodu materiālu un cieto elektrolītu sintēze un izpēte

Antonija Dindune[1], Jānis Ronis[1], Dagnija Valdniece[1], Antanas Orliukas[2],
Tomas Salkus[2], Vilma Venckute[2]
1 – Faculty of Materials Science and Applied Chemistry, Riga Technical University
Paula Valdena iela 3/7, Riga, LV-1048, Latvia
2 – Department of Radiophysics, Faculty of Physics, Vilnius University
Saulėtekio ave. 3, Vilnius, LT-10222, Lithuania
E-mail: *antonija.dindune@rtu.lv*

Contents

2.1. Introduction

Investigated NASICON-type materials can be used as charge separators for solid electrolyte batteries. Also, pyrophosphate and olivine materials can serve as cathode materials for lithium, sodium solid electrolyte batteries. The NASICON crystallographic structure $NaA_2^{IV}(PO_4)_3$ (A^{IV} = Ge, Ti and Zr) was identified in 1968 [1, 2]. The structure can be described as a covalent skeleton $[A_2P_3O_{12}]^-$ constituted of AO_6 octahedra and PO_4 tetrahedra, which form 3D interconnected channels and two types of interstitial positions (M′ and M″) where conductor cations are distributed. The conductor cations move from one site to another through bottlenecks, the size of which depends on the nature of the skeleton ions and on the carrier concentration in both type of sites (M′ and M″) Consequently, the structural and electrical properties of NASICON-type compounds vary with the composition of the framework. For example, the compound family with general formula $Li_{1-4x}Ti_{2-x}M_x(PO_4)_3$ (M = Al, Ga, In, Sc) was investigated [3]. The substitution of Ti^{4+} by smaller Me^{3+} cations changed unit cell dimensions of the NASICON framework and leads the increase of ionic conductivity by about 3 orders of magnitude. The aim of this work was the preparation Li^+ (Na^+) solid electrolytes and investigation the relationship between the crystal structure, elemental composition and peculiarities of ionic transport in these materials.

Several groups of inorganic solid NASICON-type lithium ion and the sodium-ion conductors were synthesized for the investigation.

A. Lithium ion conducting NASICON-type materials is interesting in terms of solid electrolytes for Li ion batteries. The total and bulk conductivity values of $LiTi_2(PO_4)_3$ ceramic are about $2.5 \cdot 10^{-6}$ and $6.3 \cdot 10^{-5}$ Scm^{-1}, respectively [4]. In order to increase its electrical conductivity, modified NASICON-type compounds $Li_{1+4x}Ti_{2-x}(PO_4)^3$ (x = 0.2, 0.5), $Li_{1.3}Al_yY_{x-y}Ti_{1.7}(PO_4)_3$ (x = 0.3; y = 0.1, 0.2), $Li_{1+4x}Ti_{2-x}Nb_yP_{3-y}O_{12}$ (x = 0.1, 0.2, 0.3 and y = 0, 0.1, 0.2, 0.3), $Li_3Fe_{1.2}Sc_{0.75}Y_{0.05}(PO_4)_3$ were synthesized.

B. Also several cathode materials for Li ion batteries were prepared. Lately pyrophosphates gain more and more attention as possible cathode materials [5]. In this work $Li_{1-x}Fe_{1-x}Ti_xP_2O_7$ (x = 0, 0.1) and new $Li_{4x}Ti_{1-x}P_2O_7$ (x = 0, 0.06, 0.1, 0.2) pyrophosphates were synthesized. $LiFePO_4$ and $LiFePO_4/C$ cathode materials with olivine crystal structure were also obtained.

C. A further progress in development of secondary batteries for electrochemical energy storage requires the development of new ion-conducting materials. Among various alternatives to the Li-ion batteries, the sodium-ion batteries are promising as attractive cathode materials due to the abundant resources and the low cost of sodium [6]. We continue to search for new Na-based pyrophosphate materials for application in the secondary sodium ion batteries. Powders were synthesized by solid state reaction $Na_2Zn_{0.5}Mn_{0.5}P_2O_7$, $NaCsZn_{0.5}Mn_{0.5}P_2O_7$, $Na_2MnP_2O_7$ [7, 8].

2.2. Experiments: Technologies and research methods of synthesis

Lithium and sodium solid electrolytes were synthesized and their ceramics were sintered. The powders of investigated compounds were synthesized by solid state reaction. Solid phase starting materials are used for this method of synthesis. The starting materials are mixed together and milled. Milling was performed in ethanol. Several milling and heating steps ensure that all the starting materials will come into contact with each other for reaction. The sequences of synthesis of some investigated compounds are shown below (see Fig. 2.1–2.6).

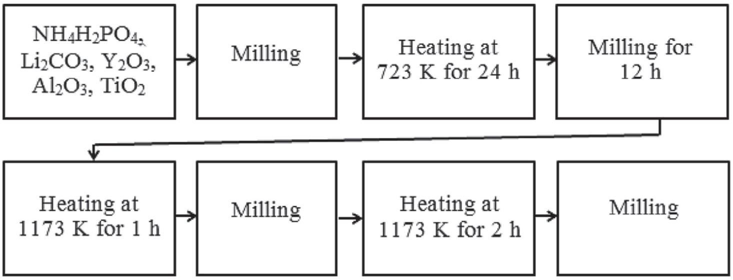

Figure 2.1. **Synthesis of $Li_{1.3}Al_yY_{x-y}Ti_{1.7}(PO_4)_3$ by solid state reaction**

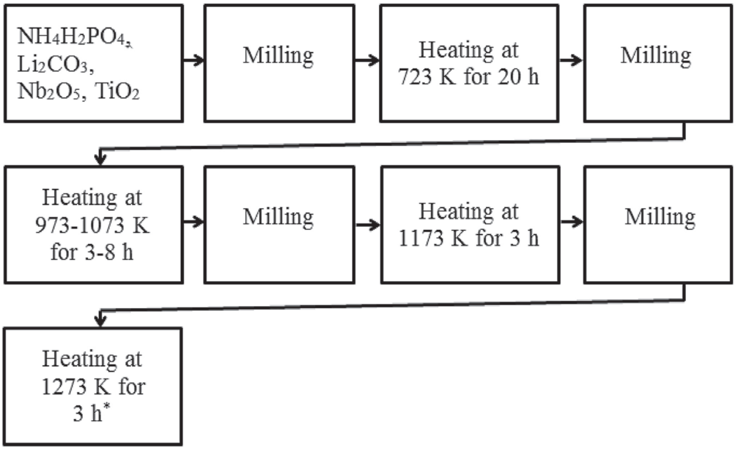

Figure 2.2. **Synthesis of $Li_{1+4x}Ti_{2-x}Nb_yP_{3-y}O_{12}$ by solid state reaction**

* The heating step for the compound with y = 0.1 was 1473 K for 2 h

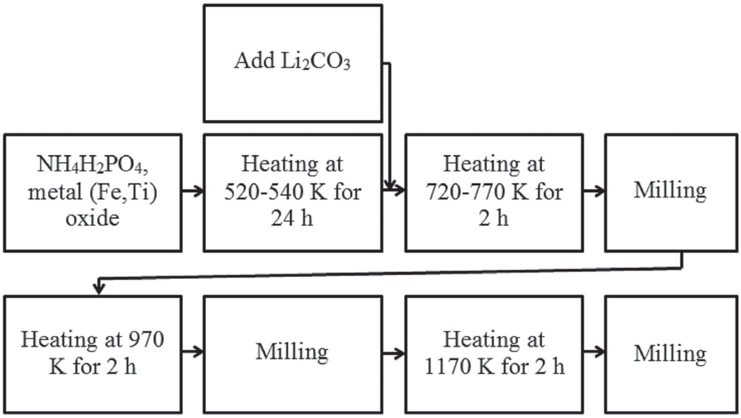

Figure 2.3. **Synthesis of $LiFeP_2O_7$ and $Li_{0.9}Fe_{0.9}Ti_{0.1}P_2O_7$ by solid state reaction**

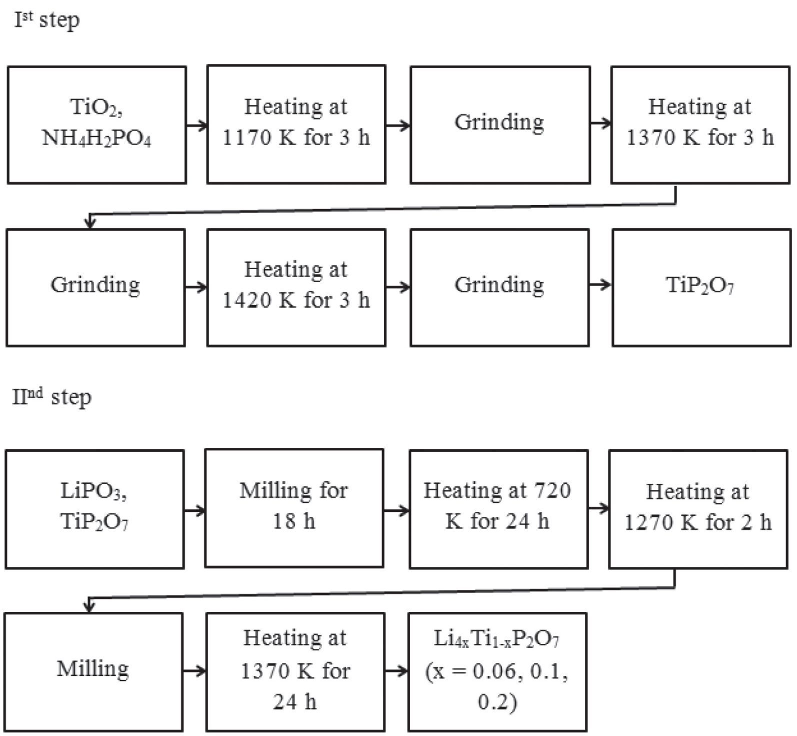

Figure 2.4. **Synthesis of $Li_{4x}Ti_{1-x}P_2O_7$ (x = 0, 0.06, 0.1, 0.2) by solid state reaction**

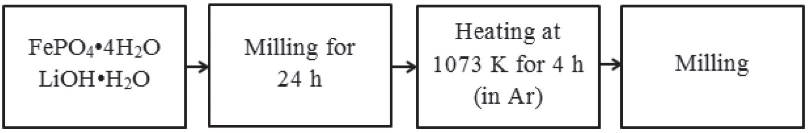

Figure 2.5. **Synthesis of $LiFePO_4$ by solid state reaction**

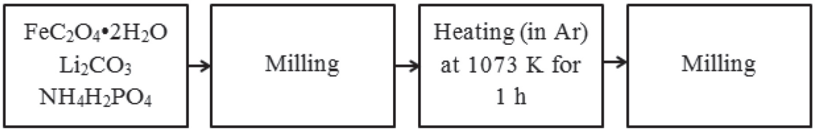

Figure 2.6. **Synthesis of $LiFePO_4$/C by solid state reaction**

Solid electrolyte ceramics fabrication technology: In order to prepare ceramics, powders of solid electrolytes were uniaxially cold-pressed into pellets at pressures between 150–300 MPa. Most pellets were sintered in air. Sintering temperatures (*T*s) and sintering times (*t*s) are presented in Table 2.1. The heating and cooling rate in the furnace was 5 K/min.

Before sintering pellets are heated at 673 K for 1 h. Densities of the pellets (d) were evaluated by measuring geometry and mass of the pellets. Relative densities of the ceramics were calculated according to formula $d_r = (d/d_{XRD})\cdot 100\%$, where d_{XRD} is the theoretical density calculated from XRD patterns of the compounds. Relative densities of the investigated ceramics are also presented in Table 2.1.

Table 2.1. **Preparation conditions and relative densities of ceramics**

Compounds	Pressure P, Pa	Sintering temperature T_s, K	Sintering time t_s, h	Relative density d_r, %
$Li_{1.8}Ti_{1.8}(PO_4)_3$	300	1363	1	95
$Li_3Ti_{1.5}(PO_4)_3$	300	923	1	81
$Li_{1.4}Ti_{1.9}P_3O_{12}$	300	1343	1	
$Li_{1.4}Ti_{1.9}Nb_{0.1}P_{2.9}O_{12}$	300	1223	1	
$Li_{1.8}Ti_{1.8}Nb_{0.2}P_{2.8}O_{12}$	300	1223	1	
$Li_{2.2}Ti_{1.7}Nb_{0.3}P_{2.7}O_{12}$	300	1223	1	
$Li_{1.3}Al_{0.2}Y_{0.1}Ti_{1.7}(PO_4)$	300	1373	1	
$Li_{1.3}Al_{0.1}Y_{0.2}Ti_{1.7}(PO_4)$	300	1373	1	
$LiFePO_4$	300	1073	10	85.8
$LiFePO_4/C$	300	1073 (in Ar)	1	73.7
$Li_4Ti_5O_{12}$	150	1173	10	79
$Li_4Ti_{4.95}Ta_{0.05}O_{12}$	150	1173	10	86
$Li_4Ti_{4.95}Nb_{0.05}O_{12}$	150	1173	10	83
$LiFeP_2O_7$	300	1173	2	73
$Li_{0.9}Fe_{0.9}Ti_{0.1}P_2O_7$	300	1173	2	71
TiP_2O_7	150	1460	3	92
$Li_{0.24}Ti_{0.94}P_2O_7$	150	1370	1	
$Li_{0.4}Ti_{0.9}P_2O_7$	150	1270	1	
$Li_{0.8}Ti_{0.8}P_2O_7$	150	1170	1	

Structural peculiarities of the compounds were investigated, using X-ray diffraction technique (XRD). For the investigations of electrical properties, the ceramic samples were sintered. The ceramic samples were investigated by using Impedance Spectroscopy (IS) in broad frequency range and temperature interval. Surfaces of the ceramics were investigated with X-ray Photoelectron Spectroscopy (XPS), Scanning Electron Microscopy

(SEM) and Energy dispersive X-ray Spectroscopy (EDX). The investigation of iron valents' state in some materials with Fe was performed, using Mössbauer spectroscopy method.

X-ray diffraction (XRD). Structural investigation of the materials was carried out with X-ray diffraction (XRD) technique. The structure parameters at room temperature were obtained from the X-ray powder diffraction, using Brucker D8 Advance equipment in the region 2 Theta = 10–70 degrees, step 0.01–0.02 degrees, time per step 1–8 sec., CuKα_1 radiation. The lattice parameters were deduced by fitting the XRD patterns with software TOPAS v. 4.1 and SCANIX v. 2.16 (Matpol).

Impedance Spectroscopy (IS). The electrical properties of the ceramics were investigated by broadband impedance spectroscopy. Measurements of complex electrical conductivity ($\tilde{\sigma} = \sigma' + i\sigma''$), complex impedance ($\tilde{\rho} = \rho' - i\rho''$) and complex dielectric permittivity ($\tilde{\varepsilon} = \varepsilon' - i\varepsilon''$) of the ceramics were carried out in air in the temperature interval from room temperature (RT) to 780 K and in the frequency range from 10 Hz to 3 GHz. The impedance spectrometer was used for the electrical measurements in the low frequency range up to 2 MHz by the 2- and 4-probe method [9], while in the microwave region a setup with a coaxial line connected to the Agilent E5062A network analyser was used [10]. Platinum paste (Gwent Electronics Materials Ltd.) was used to prepare electrodes on investigated samples.

X-ray Photoelectron Spectroscopy (XPS) or Electron Spectroscopy for Chemical Analysis (ESCA) is a powerful method of surface analysis. It collects information about surface layer of approximately 10 nm. In this work, XPS were recorded by LAS-3000 (ISA-Riber) surface analysis equipment. The instrument was equipped with double-pass cylindrical mirror analyser MAC2.

Scanning electron microscopy (SEM) and energy-dispersive X-ray spectroscopy (EDX) techniques were used for the analysis of chemical composition of the investigated compounds. Both techniques are integrated in TM3000 – Hitachi equipment, which was used for the investigation. Ceramics were prepared for SEM/EDX investigation. Pellets were broken and measurements were performed on the broken edge.

Mössbauer spectra were recorded with a conventional constant acceleration spectrometer in the transmission geometry. The density of the absorber was about 10 mg/cm^2 of natural Fe. The Co(Rh) source with the activity of 5 mCi was held at room temperature. The closed cycle helium Mössbauer cryostat (ARS Inc.) was used for the measurements at 10 K – 350 K. The Mössbauer furnace (WissEl GmbH) was used for the measurements at 300 K – 600 K. The temperature values during the measurements were kept at around the set point with the 1 % precision. The velocity scale was calibrated using the magnetic sextet of a high-purity iron foil absorber as the standard. The line width obtained for the 25 μm iron foil was 0.26±0.02mm/s at ambient temperature. All the experimental spectra were fitted using Lorentzian lines by the least-squares method using a commercially available WinNormos package in IgorPro 5.05A environment. All isomer shifts reported in this work refer to the ^{57}Co(Rh) source at a room temperature [11].

2.3. Structure and lithium ion transport in NASICON-type solid electrolytes

Structure of the investigated lithium solid electrolytes was investigated by X-Ray diffraction analysis. Refined lattice parameters and theoretical densities at room temperature are presented in Table 2.2.

Table 2.2. **Lattice parameters and theoretical densities of the powders**

Compound	Space group	a, Å	b, Å	c, Å	V, Å^3	d_{XRD} g/cm^3	Z
$Li_{1.8}Ti_{1.8}(PO_4)_3$	$R\bar{3}c$	8.5162(4)		20.8482(30)	1309.5	2.9	6
$Li_3Ti_{1.5}(PO_4)_3$	$R\bar{3}c$	8.5144(5)		20.8762(60)	1310.8	2.85	6
$Li_{1.4}Ti_{1.9}P_3O_{12}$	$R\bar{3}c$	8.5137(2)		20.8587(5)	1309.36	2.93	6
$Li_{1.4}Ti_{1.9}Nb_{0.1}P_{2.9}O_{12}$	$R\bar{3}c$	8.5267(23)		20.8608(53)	1313.49	2.97	6
$Li_{1.8}Ti_{1.8}Nb_{0.2}P_{2.8}O_{12}$	$R\bar{3}c$	8.5257(6)		20.8975(35)	1315.49	3	6
$Li_{2.2}Ti_{1.7}Nb_{0.3}P_{2.7}O_{12}$	$R\bar{3}c$	8.5242(7)		20.8976(27)	1315.04	3.03	6
$Li_{1.3}Al_{0.2}Y_{0.1}Ti_{1.7}(PO_4)_3$	$R\bar{3}c$	8.5054(4)		20.8247(12)	1304.68	2.974	6
$Li_{1.3}Al_{0.1}Y_{0.2}Ti_{1.7}(PO_4)_3$	$R\bar{3}c$	8.5109(4)		20.8372(16)	1307.1	3.016	6
$LiFePO_4$	Pnma					3.6	
$LiFePO_4/C$	Pnma					3.42	
$Li_4Ti_5O_{12}$	$Fd\bar{3}m$	8.3586			584.004	3.48	
$Li_4Ti_{4.95}Ta_{0.05}O_{12}$	$Fd\bar{3}m$	8.3627			584.85	3.48	
$Li_4Ti_{4.95}Nb_{0.05}O_{12}$	$Fd\bar{3}m$	8.3633			584.98	3.48	
$LiFeP_2O_7$	$P2_1$	4.8240(2)	8.0828(3)	6.9390(2)	255.19	3.081	
$Li_{0.9}Fe_{0.9}Ti_{0.1}P_2O_7$	$P2_1$	4.8239(4)	8.0786(6)	6.9365(5)	255.09	3.063	
TiP_2O_7	$Pa\bar{3}$	23.6249(2)				3.015	108
$Li_{0.24}Ti_{0.94}P_2O_7$	$Pa\bar{3}$	23.6229(2)				3	108
$Li_{0.4}Ti_{0.9}P_2O_7$	$Pa\bar{3}$	23.6235(2)				2.99	108
$Li_{0.8}Ti_{0.8}P_2O_7$	$Pa\bar{3}$	23.6262(2)				2.96	108

NASICON-type structure compounds. Fig. 2.7 shows powder X-ray diffraction patterns of $Li_{1.3}Al_yY_{x-y}Ti_{1.7}(PO_4)3$(x = 0.3; y = 0.1, 0.2) prepared by solid state reaction. Small amounts (up to 1.5 %) of $LiTiPO_5$ and YPO_5 were detected as impurities and marked with asterisks in Fig. 2.7. At the room temperature, the $Li_{1.3}AlyY_{x-y}Ti_{1.7}(PO4)_3$(x = 0.3; y = 0.1, 0.2) compounds belong to the rhombohedral symmetry (space group *R3 c*) with six formula units in the unit cell [13]. The lattice parameters, unit cell volume (*V*) and theoretical density (*d*t) of the investigated compounds are presented in Table 2.2.

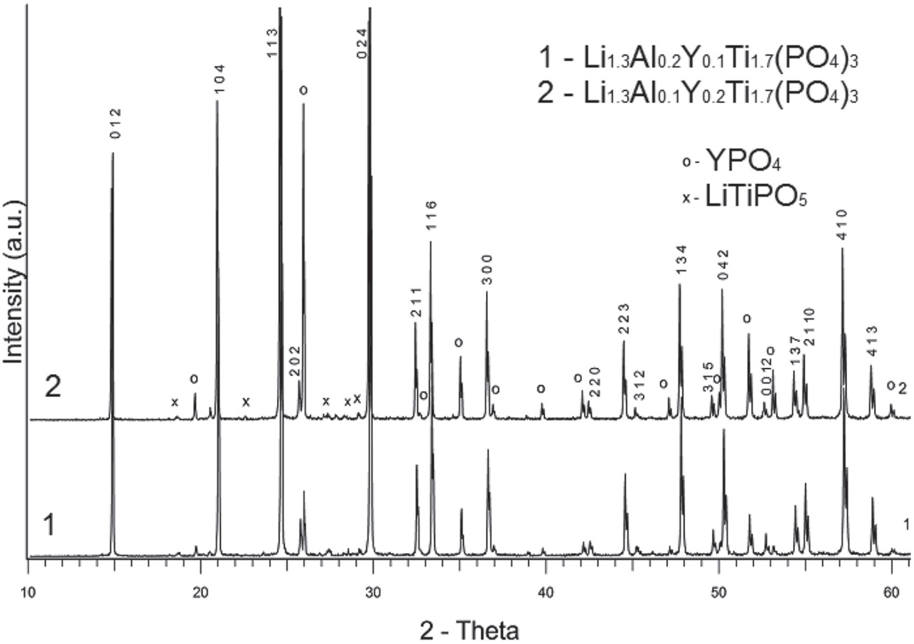

Figure 2.7. **Powder X-ray diffraction patterns of $Li_{1.3}Al_yY_{x-y}Ti_{1.7}(PO_4)_3$ (x = 0.3; y = 0.1, 0.2) recorded at room temperature**

A partial substitution of $Al^{3+}$by Y^{3+}in $Li_{1.3}Al_yY_x-_yTi_{1.7}(PO_4)_3$ (x = 0.3; y = 0.1, 0.2) causes the increase in the lattice parameters and theoretical density of the compound. This variation can be caused by different ionic radii of $Y^{3+}$and Al^{3+}ions. The ionic radii of $Y^{3+}$and $Al^{3+}$are 1.04 Å and 0.675 Å, respectively. On the other hand, the analysis of XRD patterns shows impurities of YPO_4 and $LiTiPO_5$, which can influence the above-mentioned parameters.

Fig. 2.8 shows powder X-ray diffraction patterns of $Li_{1+4x}Ti_{2-x}Nb_yP_{3-y}O_{12}$ (x = 0.1, 0.2, 0.3; y = 0, 0.1, 0.2, 0.3) compounds. The results of XRD data analysis have shown that $LiTiPO_5$ impurities are present in compounds with y = 0, 0.1, 0.2, and they are marked with asterisks. In compounds with y = 0, 0.1, 0.2 the amounts of impurities were found to be 2%, 3%, 8%, respectively. The investigated compounds belong to hexagonal symmetry (space group R c). The lattice parameters, unit cell volume (*V*), theoretical density ($d_{x\text{-}ray}$) and formula units in the lattice (*Z*) of the investigated compounds are presented in Table 2.2. The relative density of the ceramics was found to be 94 % of the theoretical density [12].

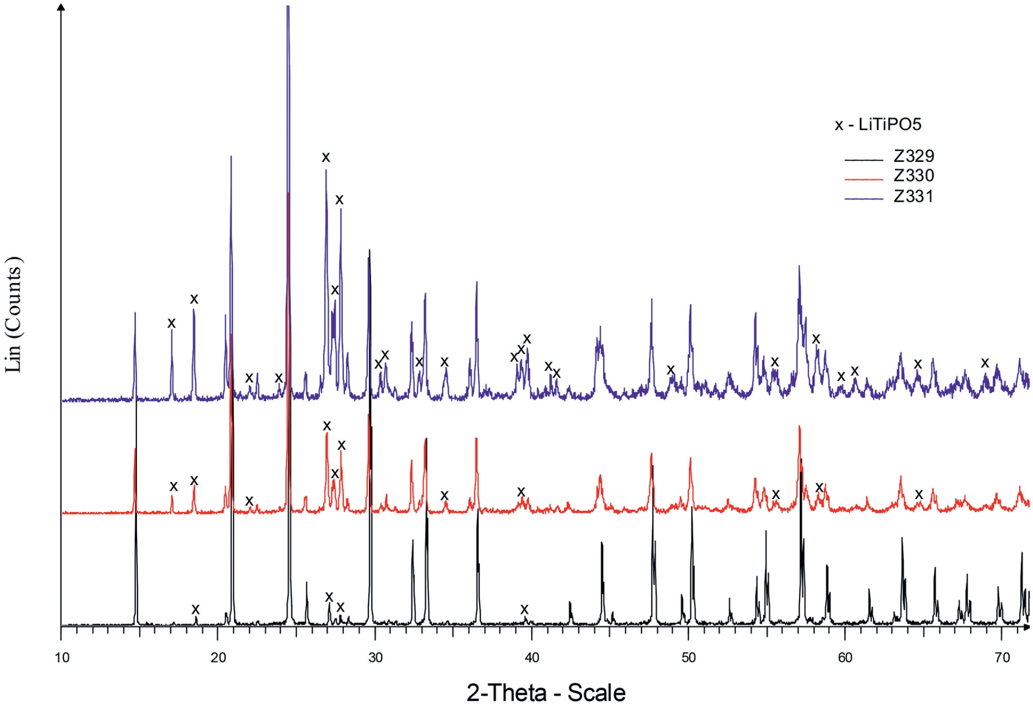

Figure 2.8. **The powder X-ray diffraction patterns of $Li_{1+4x}Ti_{2-x}Nb_yP_{3-y}O_{12}$ compounds:**
$Li_{1.4}Ti_{1.9}P_3O_{12}$ (x = 0.1, y = 0) – (black),
$Li_{1,4}Ti_{1,9}Nb_{0,1}P_{2,9}O_{12}$ (x = 0.1, y = 0.1) – (red),
$Li_{1.8}Ti_{1.8}Nb_{0.2}P_{2.8}O_{12}$ (x = 0.2, y = 0.2) – (blue)

The amounts of up to 0.8 wt. % and 5 wt. % of $LiTiPO_5$ and $Li_4(P_2O_7)$ in compounds $Li_{1+4}xTi_{2-x}(PO_4)_3$with x = 0.2 and 0.5, respectively, were found. The amounts of impurities were estimated from the intensities and their square analysis of XRD patterns. $LiTiPO_5$ and $Li_4(P_2O_7)$ belong to orthorhombic and triclinic symmetry group and are marked with asterisks on the XRD patterns in Fig. 2.9. At room temperature the $Li_{1+4}xTi_{2-x}(PO_4)_3$(where x = 0.2, 0.5) compounds belong to the rhombohedral symmetry (space group *R* 3 *c*) with six formula units in the unit cell. The lattice *a*, *c* parameters, volume (*V*), theoretical density (*d*t) of the ceramics are presented in Table 2.2.

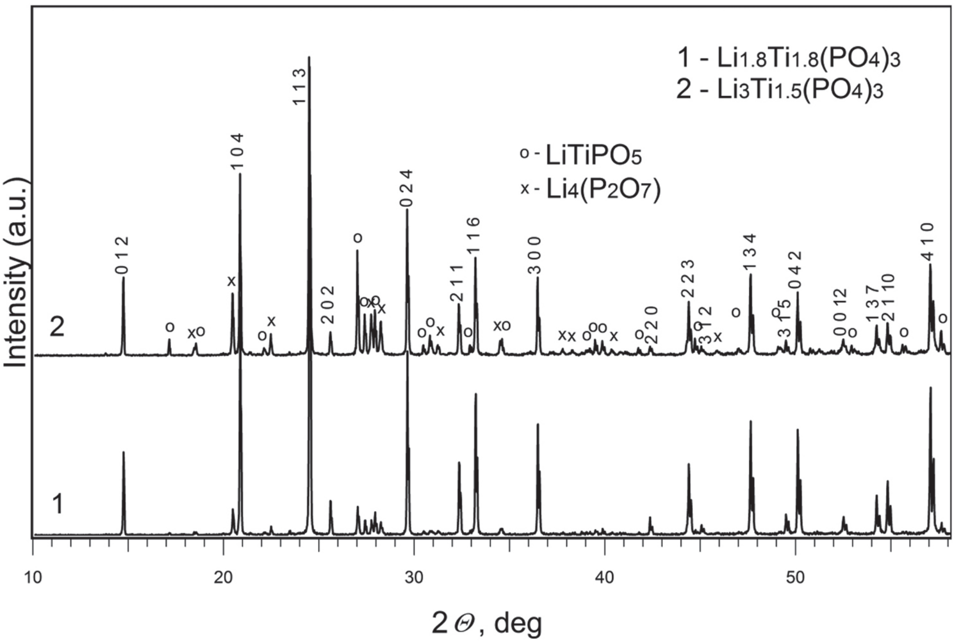

Figure 2.9. **XRD patterns of $Li_{1+4x}Ti_{2-x}(PO_4)_3$ (where x = 0.2, 0.5) at room temperature**

The increase of Li content (Fig. 2.9) leads to the increase of volume of the lattice and decrease of the theoretical density of the compounds. This variation can be caused by the different values of the ionic radii of Li^+ and Ti^{4+} ions. The ionic radii of Li^+ and Ti^{4+} are 0.92 Å and 0.74 Å, respectively. On the other hand, the analysis of XRD patterns shows the impurities of LiTiPO5 and $Li_4(P_2O_7)$, which can also influence the above-mentioned parameters [14].

XRD spectra of $LiFeP_2O7$ and $Li_{0.9}Fe_{0.9}Ti_{0.1}P_2O_7$ pyrophosphates at various temperatures

X-ray powder diffraction analysis was performed at temperatures T = 300, 440, 540 and 680 K. The X-ray diffraction patterns of [15] $LiFeP_2O_7$ and $Li_{0.9}Fe_{0.9}Ti_{0.1}P_2O_7$ powders at 300 K and 680 K are presented in Fig. 2.10. Crystal structure of $LiFeP_2O_7$ powders has been indexed as monoclinic system (s.g. $P2_1$) in all the investigated temperatures. The structure of $Li_{0.9}Fe_{0.9}Ti_{0.1}P_2O_7$ powders was also indexed as monoclinic system with $P2_1$ space group. Based on the observation of the same space group and other examples of partial Fe substitution in $LiFeP_2O_7$, it is expected that Ti partially replaces Fe atoms at their original sites, but calculated and difference curves (Fig. 2.10) indicates several additional peaks and intensity discrepancies.

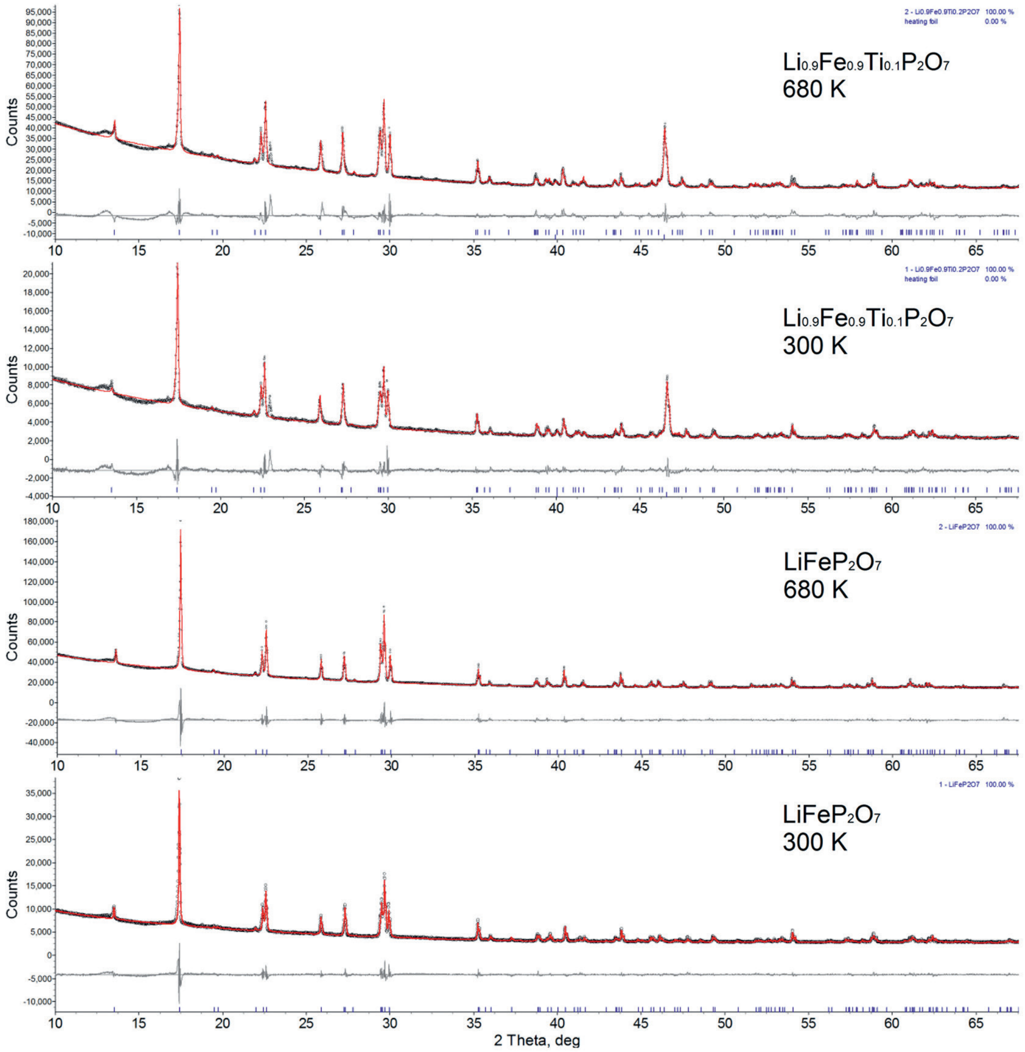

Figure 2.10. **X-ray diffraction patterns for $Li_{0.9}Fe_{0.9}Ti_{0.1}P_2O_7$ and $LiFeP_2O_7$ compounds at 300 K and 680 K temperature**

The peaks at roughly 40.0 and 46.6 degrees are known to be caused by heating element (Pt-Rh foil) and were included in the structure refinement as a Pawley phase (cubic, s. g. Fm-3 m, a ≈ 4.8242). The exact cause of the strong peak at roughly 23.00 degrees and some minor peaks (for example at 16.89, 24.49 and 26.09) is not clear, therefore, it is not presented in the refinement (Fig. 2.10.). However, it is probable that later peaks belong to the monoclinic $Fe(PO_3)_3$ phase (it could consist up to 6 wt. %), which was reported in [16]. The attempts to refine $Li_{0.9}Fe_{0.9}Ti_{0.1}P_2O_7$ XRD data using another Ti sites or other space group were not successful, therefore, despite the observed inadequacies, we assume that the structure is generally correct.

The additional modest improvement of XRD data refinement was observed after occupation coefficients (occ) were varied freely: for all atomic positions of $LiFeP_2O_7$, refined occ was close to 0.9, meanwhile, for $Li_{0.9}Fe_{0.9}Ti_{0.1}P_2O_7$ refined occ values had a tendency to be smaller by a value of 0.2–0.3 and for some sites even lower than 0.5. Variation of occ are accompanied by inadequate changes of isotropic temperature factors (beq), therefore, in the presented XRD data refinement variation of beq was limited (the chosen variation range limits were from 0 to 1). Under such restrictions, beq relaxed to values close to 0 and 1: for $LiFeP_2O_7$ at 300 K beq relaxed to value of 0 only for Lithium and two oxygen atomic sites (four oxygen sites at 680 K); for $Li_{0.9}Fe_{0.9}Ti_{0.1}P_2O_7$ at 300 K beq relaxed to value of 0 for iron, lithium and two oxygen sites; for $Li_{0.9}Fe_{0.9}Ti_{0.1}P_2O_7$ 680 K beq relaxed to value of 0 for lithium and six oxygen sites. Both of these effects (occ and beq variations) could be caused by the insufficient data quality, which is reduced due to possible changes of heating foil curvature, X-ray beam cropping and scattering by heating chamber windows, relatively small acquisition times. On the other hand, the anomalies of lattice parameters and tendency of occ changes of the atoms in the both compounds can be related to disordering in the unit cells of the compounds. This assumption is also supported by the observed differences in P/Fe atomic concentration ratios and variations of Fe^{2+} and Fe^{3+} states.

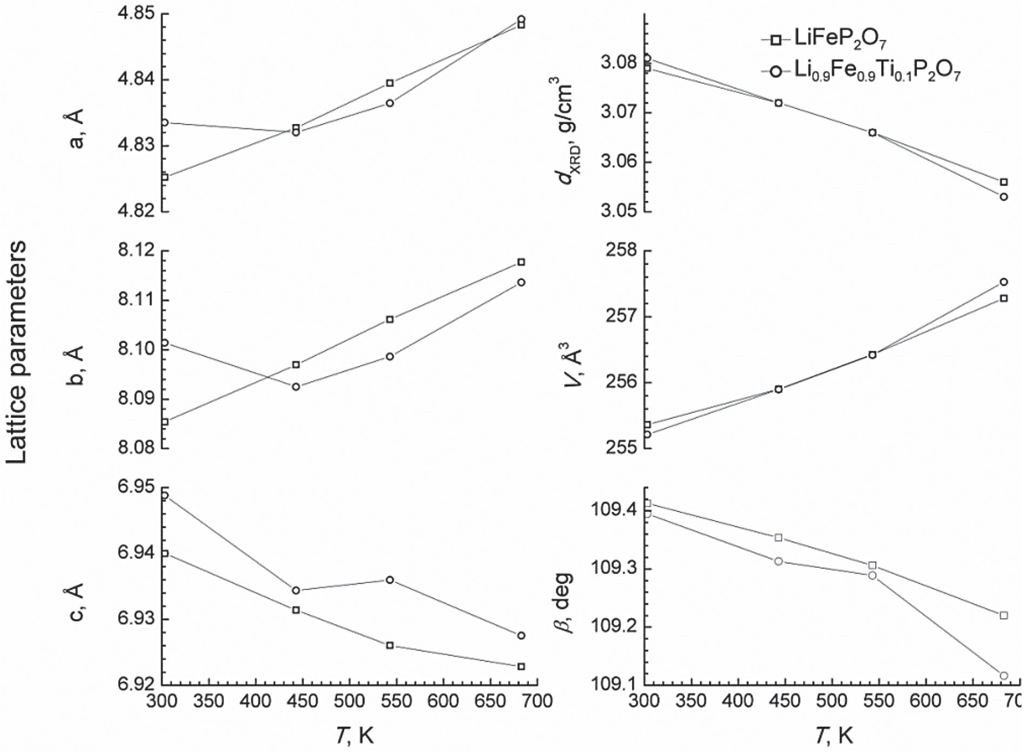

Figure 2.11. **Lattice parameters (a, b, c), angle (β), volume (V), theoretical density (d_{XRD}) of $Li_{0.9}Fe_{0.9}Ti_{0.1}P_2O_7$ and $LiFeP_2O_7$ compounds determined from XRD analysis at different temperatures**

The refined lattice (a, b, c) parameters, volume of the unit cell (V), theoretical (d_{XRD}) density of the ceramics at room temperature are summarized in Table 2.2. The temperature dependences of the lattice parameters, V, β of the investigated compounds are shown in Fig. 2.11. The volumes of the cells increase, β and densities decrease with increase of the temperature. The anomalies of lattice parameters of $LiFeP_2O_7$ and $Li_{0.9}Fe_{0.9}Ti_{0.1}P_2O_7$ in the temperature range 543 to 680 K were found. The anomalies of lattice parameters in the both compounds can be related to disordering in the unit cells of the compounds. It is worth to note, that the space group of both compounds at 300 K and 683 K temperature remains the same.

Crystal structure of $Li_{4x}Ti_{1-x}P_2O_7$ (x = 0, 0.06, 0.1, 0.2) pyrophosphates. XRD analysis at room temperature confirmed that obtained $Ti_2P_2O_7$ powder belongs to cubic symmetry with space group $Pa\bar{3}$ as Results of X-ray diffraction analysis also show that $Li_{4x}Ti_{1-x}P_2O_7$(x = 0.06, 0.1, 0.2) compounds have cubic superstructure and the same space group as $Ti_2P_2O_7$. The obtained XRD patterns are shown in Fig. 2.12. The increase of lithium amount in the system $Li_{4x}Ti_{1-x}P_2O_7$ slightly decreased the theoretical density of the compounds (see Table 2.2).

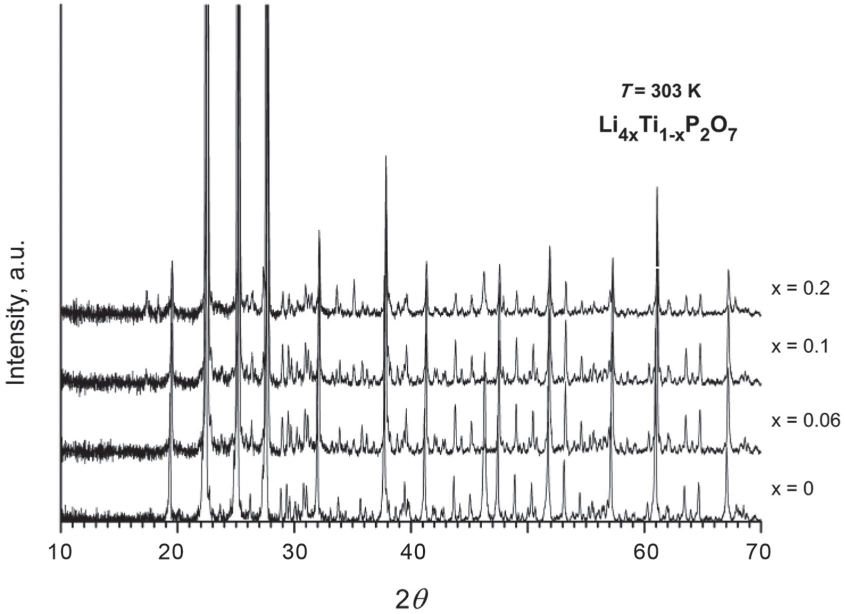

Figure 2.12. **X-ray diffraction patterns of $Li_{4x}Ti_{1-x}P_2O_7$ (where x = 0, 0.06, 0.1, 0.2) powders**

2.4. Electrical properties of NASICON-type compounds

The impedance spectroscopy investigation of the ionic conductivity in the wide frequency and in the broad temperature ranges allows to separate charge carrier transport processes in bulk and in grain boundaries of the ceramics. The results of the investigation of electrical conductivities have shown [**13**] that the increase of stoichiometric parameter y in $Li_{1.3}Al_yY_{x-y}Ti_{1.7}(PO_4)_3$ (x = 0.3; y = 0, 0.1, 0.15, 0.2, 0.3) system leads to the increase of σ_b values (see Fig. 2.13 and Table 2.3).

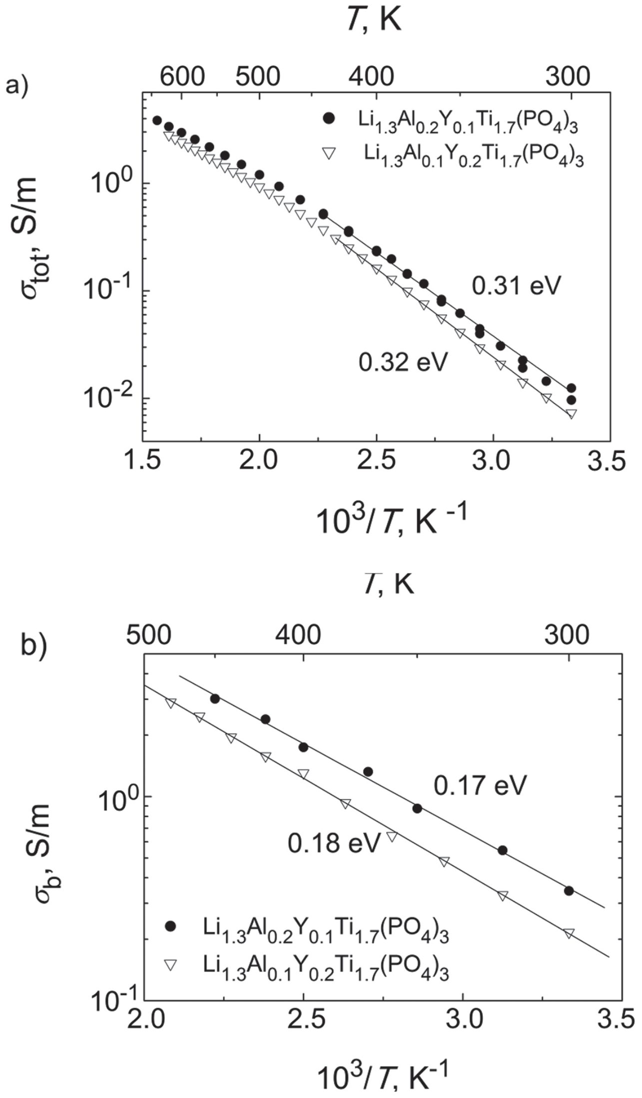

Figure 2.13. **Temperature dependences of total (a) and bulk (b) conductivities of $Li_{1.3}Al_yY_{x-y}Ti_{1.7}(PO_4)_3$ (x = 0.3; y = 0.1, 0.2) ceramics**

Table 2.3. **σ_b, σ_{tot}, their activation energies and activation energy of the relaxation frequency in bulk of $Li_{1.3}Al_yY_{x-y}Ti_{1.7}(PO_4)_3$ (x = 0.3; y = 0, 0.1, 0.15, 0.2, 0.3) ceramic samples at 300 K**

Compounds’	σ_b S/m	$\Delta E_{\sigma b}$, eV	ΔE_f, eV	σ_{tot}, S/m	$\Delta E_{\sigma tot}$, eV	Ref.
$Li_{1.3}Al_{0.3}Ti_{1.7}(PO_4)_3$	0.35	0.30	0.30			[17]
$Li_{1.3}Al_{0.2}Y_{0.1}Ti_{1.7}(PO_4)_3$	0.35	0.17	0.18	0.012	0.32	
$Li_{1.3}Al_{0.15}Y_{0.15}Ti_{1.7}(PO_4)_3$	0.22	0.26	0.26	0.0019	0.45	[18]
$Li_{1.3}Al_{0.1}Y_{0.2}Ti_{1.7}(PO_4)_3$	0.22	0.18	0.17	0.0073	0.31	
$Li_{1.3}Y_{0.3}Ti_{1.7}(PO_4)_3$	0.094	0.19	0.19			[17]

A good agreement between the activation energy of ionic migration process in grains, $\Delta E\sigma_b$, and the activation energy of characteristic relaxation frequency, ΔE_f, is found. The activation energy ΔE_f correlates with the activation energy of mobility of charge carriers in grains. As we found that the values of activation energies of the bulk ionic conductivities of investigated ceramics are similar to the activation energies of relaxation frequency, which can be attributed to migration of Li^+ ions, the concentration of charge carriers remains constant with changing temperature. It is shown that the major role in the temperature dependence of bulk conductivity is played by the Li^+ ion mobility, which increases as temperature increases.

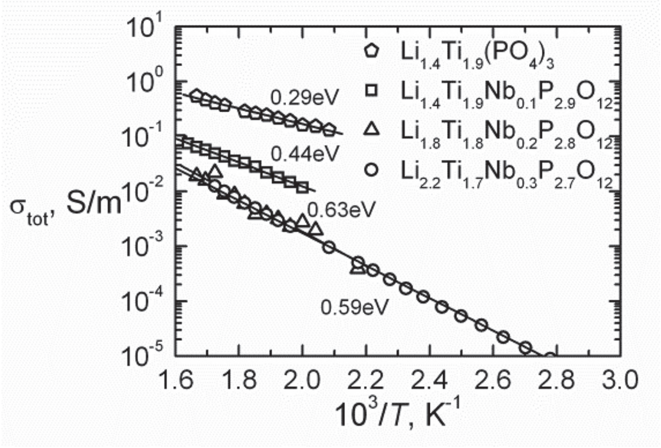

Figure 2.14. **Temperature dependences of total conductivities of $Li_{1+4x}Ti_{2-x}Nb_yP_{3-y}O_{12}$ ceramics**

Electrical properties of $Li_{1+4x}Ti_{2-x}Nb_yP_{3-y}O_{12}$ ceramics were investigated by using two probe methods. Two relaxation dispersions have been found in complex conductivity and impedance spectra of the studied $Li_{1+4x}Ti_{2-x}Nb_yP_{3-y}O_{12}$ ceramics. The one in the high frequency region was attributed to Li^+ ion relaxation in the bulk, and the intermediate frequency range dispersion was caused by ion blocking effect at grain boundaries of the ceramics [**12**]. Temperature dependences of σ_{tot} of $Li_{1+4x}Ti_{2-x}Nb_yP_{3-y}O_{12}$ (x = 0.1, 0.2, 0.3; y = 0, 0.1, 0.2, 0.3) ceramics are shown in Fig. 2.14. σ_b and σ_{tot} of investigated ceramics change according to Arrhenius law in the studied temperature range. The values of σ_b and σ_{tot}, their activation energies (ΔEb) and (ΔEtot) are summarized in Table 4. The comparison of the results of the XRD and conductivity investigations has shown that the increase of impurities of $LiTiPO_5$ leads to the decrease of total and bulk conductivities and increase their activation energies. According to [19], the compound of $LiTiPO_5$ exhibit very low electrical conductivity ((5–10).10^{-4} S/m at 673 K, its activation energy $\Delta E \approx 1$ eV).

Table 2.4. **σ_b and σ_t, and their activation energies of $Li_{1+4x}Ti_{2-x}Nb_yP_{3-y}O_{12}$ ceramics at temperature T = 530 K**

Compounds	S_b, S·m^{-1}	ΔE_b,eV	S_t,S·m^{-1}	ΔE_t,eV
$Li_{1.4}Ti_{1.9}P_3O_{12}$	2.07	0.18	0.244	0.29
$Li_{1.4}Ti_{1.9}Nb_{0.1}P_{2.9}O_{12}$	0.22	0.38	0.022	0.44
$Li_{1.8}Ti_{1.8}Nb_{0.2}P_{2.8}O_{12}$	0.05	0.4	0.004	0.59
$Li_{2.2}Ti_{1.7}Nb_{0.3}P_{2.7}O_{12}$	0.04	0.43	0.0038	0.59

$Li_{1+4x}Ti_{2-x}(PO_4)_3$ (where x = 0.2, 0.5) ceramics measured in the frequency range from 10 Hz to 100 kHz were investigated by four probe method and in the microwave range the measurements were carried out by coaxial technique.

The temperature dependences of bulk ionic conductivities (σ_b) have been found from complex plain plots of conductivity at different temperatures. The temperature dependences of σ_b and σ_{tot} of $Li_{1+4x}Ti_{2-x}(PO_4)_3$ (where x = 0.2, 0.5) of ceramic samples are shown in Fig. 2.15. The maximal value of σ_{tot} was found for compound with parameter x = 0.5. The increase of the parameter x leads to the increase of the value of σ_b. The activation energies of σ_b and σ_{tot} were found from the slopes of the Arrhenius plots.

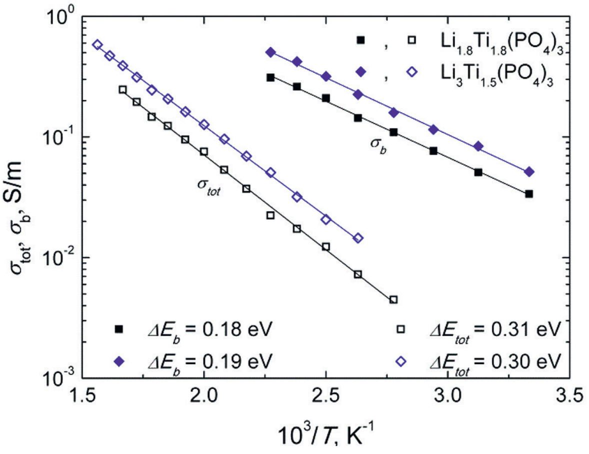

Figure 2.15. **Arrhenius plots of total and bulk conductivities of $Li_{1+4x}Ti_{2-x}(PO_4)_3$ (where x = 0.2, 0.5) ceramics**

2.5. Anomalies of electrical properties of $LiFeP_2O_7$ and $Li_{0.9}Fe_{0.9}Ti_{0.1}P_2O_7$ pyrophosphate ceramics

The characteristic frequency dependences of the real part of complex conductivity of the $LiFeP_2O_7$ and $Li_{0.9}Fe_{0.9}Ti_{0.1}P_2O_7$ ceramics were measured at temperatures 560 K and 660 K [15, 20]. The dispersion regions in spectra for both investigated ceramics were found. The processes are thermally activated and dispersion regions shift towards higher frequencies as temperature increases. This phenomenon is typical for relaxation-type dispersions, which are general in the solid electrolyte ceramics [21, 22]. It was not possible to distinguish grain boundary and bulk conductivities of the ceramics in the measured temperature and frequency ranges, as they were separated in the previous works [23, 24].

The total conductivities σ_{tot} of the ceramics were derived from frequency dependences at different temperatures and complex specific resistance. The temperature dependences of σ_{tot} of $LiFeP_2O_7$ and $Li_{0.9}Fe_{0.9}Ti_{0.1}P_2O_7$ ceramic samples are shown in Fig. 2.16.

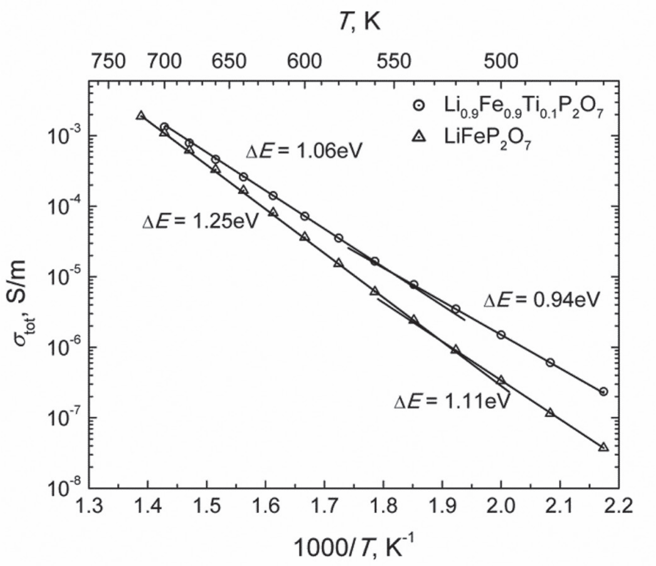

Figure 2.16. **Total conductivity of $Li_{0.9}Fe_{0.9}Ti_{0.1}P_2O_7$ and $LiFeP_2O_7$ compound ceramics dependences on reciprocal temperature**

The activation energies (ΔE) of σ_{tot} were found from the slopes of the Arrhenius plots. The partial changes of Fe^{3+} by Ti^{4+} in the compounds lead the increase of the value of σ_{tot} and decrease their activation energy of the investigated ceramics. The activation energy of σ_{tot} for $LiFeP_2O_7$ and $Li_{0.9}Fe_{0.9}Ti_{0.1}P_2O_7$ ceramics was found to be 1.11 eV and 0.94 eV respectively. At temperature $T = 550$ K for $LiFeP_2O_7$ and at $T = 528$ K for $Li_{0.9}Fe_{0.9}Ti_{0.1}P_2O_7$ compounds the change of activation energy of σ_{tot} was found. The values of ΔE of σ_{tot} above 550 K for $LiFeP_2O_7$ and above 528 K for $Li_{0.9}Fe_{0.9}Ti_{0.1}P_2O_7$ were found to be 1.25 eV and 1.06 eV, respectively. The changes of activation energy of σ_{tot} of the investigated compounds are related to structure phase transitions detected by XRD measurements. The experimental results of the investigation of σ_{tot}, their activation energies and temperatures of the changes of ΔE are summarized in Table 2.5.

Table 2.5. **Summary of electrical properties: total conductivity (σ_{tot}), activation energy (ΔE_a), Maxwell relaxation frequency (f_M), dielectric permittivity (ε'), tangent loss (tanδ) investigation at different temperatures (*T*)**

Compound	*T*, K	σtot, S/m	ΔE*a*, eV	f_M, MHz	ε'	tanδ
$Li_{0.9}Fe_{0.9}Ti_{0.1}P_2O_7$	**460-550**	$1.5{\cdot}10^{-6}$ (500 K)	0.94		6.63 (500 K)	0.0075 (500 K)
	550-700	$1.34{\cdot}10^{-3}$ (700 K)	1.06	3.28 (700 K)	7.35 (700 K)	0.049 (700 K)
$LiFeP_2O_7$	**460-528**	$3.33{\cdot}10^{-7}$ (500 K)	1.11		6.74 (500 K)	0.0074 (500 K)
	528-720	$1.09{\cdot}10^{-3}$ (700 K)	1.25	2.62 (700 K)	7.48 (700 K)	0.031 (700 K)

2.6. Influence of stoichiometry on the electrical properties of $Li_{4x}Ti_{1-x}P_2O_7$ pyrophosphate ceramics

$Li_{4x}Ti_{1-x}P_2O_7$ (x = 0, 0.06, 0.1, 0.2) samples were obtained. The temperature dependences of total conductivities σ_{tot} of the ceramics were derived from complex impedance plots obtained at different temperatures [25]. The temperature dependences of σ_{tot} are presented in Fig. 2.17. The activation energies (ΔEtot) of σ_{tot} were calculated according to Arrhenius law. The anomalies of activation energies of σ_{tot} of $Li_{4x}Ti_{1-x}P_2O_7$ (x = 0.06, 0.1, 0.2) compounds in the temperature range from 520 to 580 K were found. The changes of ΔE_{tot} can be related to some disordering in the supercell associated with phase transitions.

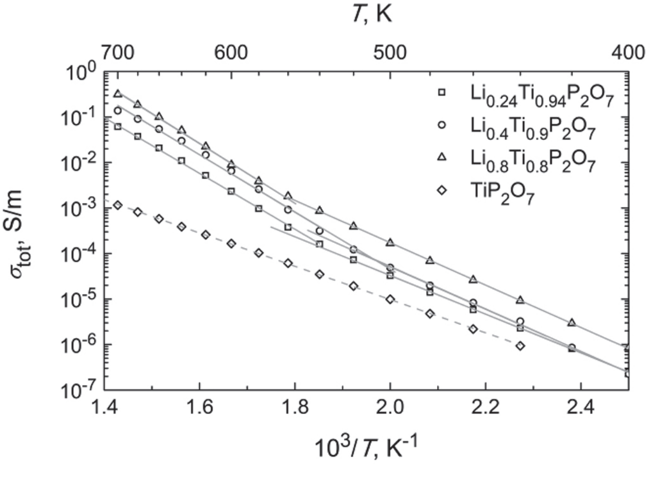

Figure 2.17. **Temperature dependences of total conductivity of $Li_{4x}Ti_{1-x}P_2O_7$ (x = 0, 0.06, 0.1, 0.2) ceramics**

The results of the investigation of σ_{tot} are summarized in Table 2.6. The values of total conductivity are higher for the samples with lithium ($Li_{4x}Ti_{1-x}P_2O_7$, x = 0.06, 0.1, 0.2) than for the host TiP_2O_7 compound (see Table 2.6). With increasing amount of lithium in the samples, σ_{tot} values also increase. The increase of the values of total conductivity in $Li_{4x}Ti_{1-x}P_2O_7$ (x = 0.06, 0.1, 0.2) compared with TiP_2O_7 can be caused by lithium ion transport contribution to σ_{tot}.. The total proton conductivity of TiP_2O_7 compound increases along with temperature according to Arrhenius law with activation energy ΔE_{tot} = 0.73 eV.

Table 2.6. **Total conductivities and their activation energies of $Li_{4x}Ti_{1-x}P_2O_7$ (where x = 0, 0.06, 0.1, 0.2) ceramics**

x in $Li_{4x}Ti_{1-x}P_2O_7$	**Sintering duration**	**Total conductivity s_{tot}, S/m (440 K)**	**Activation energy DE_{tot}, eV**	**Total conductivity σ_{tot} S/m (600 K)**	**Activation energy DE_{tot}, eV**
0	3 h	$9.34{\cdot}10^{-7}$	0.73 (440–720 K)	$1.66{\cdot}10^{-4}$	
0.06	1 h	$2.29{\cdot}10^{-6}$	0.85 (400–530 K)	$2.33{\cdot}10^{-3}$	1.23 (530–720 K)
0.1	1 h	$3.24{\cdot}10^{-6}$	0.93 (400–510 K)	$6.52{\cdot}10^{-3}$	1.26 (510–700 K)
0.2	1 h	$9.12{\cdot}10^{-6}$	0.93 (400–567 K)	$8.87{\cdot}10^{-3}$	1.31 (567–700 K)

2.7. Electrical properties of $LiFePO_4$ and $LiFePO_4$/C ceramics in the broad frequency range

The characteristic frequency dependences of the real part of complex conductivity of the $LiFePO_4$ ceramics measured at different temperatures (300, 350 and 400 K). The thermally activated dispersion regions in spectra for both investigated samples were found [26].

The dispersion regions shift towards higher frequencies as temperature increases. This phenomenon is typical for relaxation type dispersions [22]. The low frequency dispersion regions can be associated with relaxation processes in the grain boundary of the ceramics. The dispersion at high frequencies is caused by ionic transport in the bulk of the ceramics.

The temperature dependences of σ_b and σ_{tot} of the $LiFePO_4$ ceramic and the $LiFePO_4$/C composite samples are shown in Fig. 2.18.

Table 2.7. **Summary of the electrical characteristic at different temperatures for $LiFePO_4$ and $LiFePO_4$/C samples**

Compound	σ_b, S/m (320 K)	ΔE_b, eV	σ_{tot}, S/m (320 K)	ΔE_{tot} eV	ε′ (1 GHz) (320 K)	tanδ (1 GHz) (320 K)	f_M, MHz (420 K)	ΔE_{fb}, eV	ΔE_{fgb}, eV
$LiFePO_4$	$3.17{\cdot}10^{-5}$	0.60	$9.3{\cdot}10^{-6}$	0.66	15.09	0.14	5.92	0.55	0.61
$LiFePO_4$/C			$1.65{\cdot}10^{-6}$	0.49				0.54	

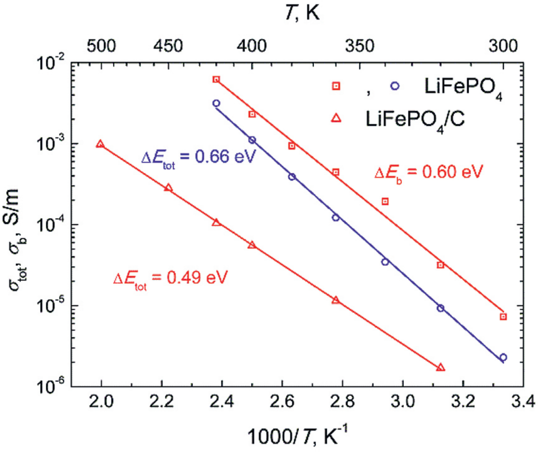

Figure 2.18. **The temperature dependences of total and bulk conductivities of the $LiFePO_4$ and the $LiFePO_4/C$ ceramics**

The activation energies of σ_{tot} (ΔE_{tot}) and of σ_b (ΔE_b) were found from the slopes of the Arrhenius plots. The experimental results of the investigation of σ_b and σ_{tot}, their activation energies are summarized in Table 2.7.

2.8. Study of the $Li_3Fe_{1.2}Sc_{0.75}Y_{0.05}(PO_4)_3$ ceramics by impedance and Mössbauer spectroscopy

Li^+ conductive NASICON type $Li_3Fe_{1.2}Sc_{0.75}Y_{0.05}(PO_4)_3$ compound has been synthesized by solid state reaction method [11, 27]. Ceramic samples were prepared for the study of electrical properties. Two and four probe methods were used for measurements of electrical impedance in the frequency range from 10 Hz to 1 MHz. Coaxial line was used for the investigation of impedance spectra in the frequency range from 1 MHz to 3 GHz. The electrical properties of the ceramics were studied in the temperature interval from room temperature (RT) to 600 K. The Mössbauer spectra were measured in the temperature interval (10–600) K (Fig. 2.19).

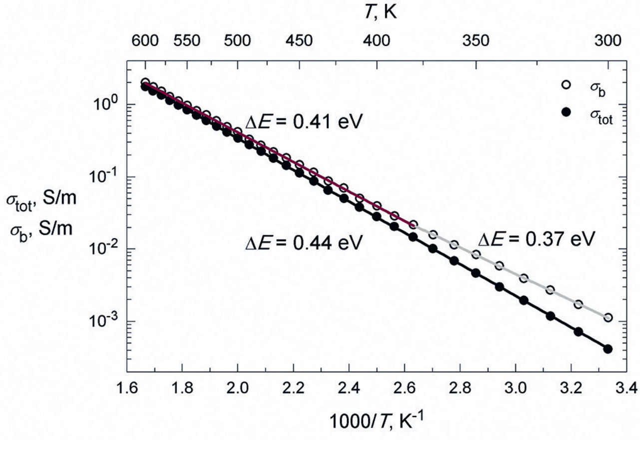

Figure 2.19. **Total (σ_{tot}) and bulk (σ_b) conductivities of $Li_3Fe_{1.2}Sc_{0.75}Y_{0.05}(PO_4)_3$ ceramics' dependences on reciprocal temperature**

The results of the investigation of the structure parameters showed that $Li_3Fe_{1.2}Sc_{0.75}Y_{0.05}(PO_4)_3$ compound was a single phase material and belonged to the monoclinic symmetry (space group $P2_1/n$) with Z = 4 formula units in the unit cell. The cell parameters a, b, c and volume (V) of the cell were found to be 8.715(4) Å, 12.181(9) Å, 8.684(3) Å and 921.90 Å^3, respectively. The theoretical density (d_t) of the compound was found to be 2.956 g/cm^3.

The value of the of total conductivity of the $Li_3Fe_{1.2}Sc_{0.75}Y_{0.05}(PO_4)_3$ ceramics at the room temperature is three times higher than the value for $Li_3Sc_{2-x}Fe_x(PO_4)_3$ (x = 0.4), and the value of grain conductivity is more than three orders of magnitude higher than that of $Li_3Sc_2(PO_4)_3$ crystals. At temperature $T = 380$ K, the change of ΔE_b was found. In the temperature range T ≥ 380 K the value of ΔE_b was found to be 0.41 eV. The ΔE_b change at 380 K can be associated with β → γ phase transition as previously was observed at higher temperatures in $Li_3Sc_{2-x}Y_x(PO_4)_3$ ($0.1 \le x \le 0.3$) system [28].

At temperature of around 380 K, the changes of activation energies of the grain conductivity, relaxation frequency were indicated also in quadrupole splitting of Mössbauer spectra (Fig. 2.20). The phenomenon can be related with β → γ phase transition in the investigated compound.

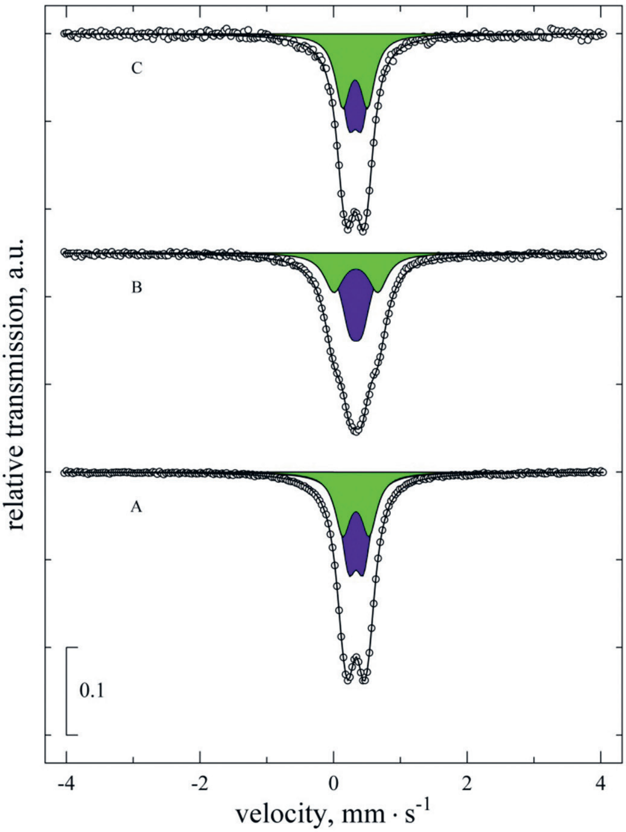

Figure 2.20. **Mössbauer spectra measured at room temperature. A – as prepared sample; B – after heating up to 578 K; C – same as B, but cooled in liquid nitrogen**

From Mössbauer spectroscopy (Fig. 2.20) it is evident that there exist two different ferric iron positions in the $Li_3Fe_{1.2}Sc_{0.75}Y_{0.05}(PO_4)_3$ compound. Hyperfine parameters of iron ions are consistent with the octahedral coordination. The changes in quadrupole splitting at 380 K are in good agreement with the observed changes in the conductivity and activation energies. As the temperature is lowered, the system shows hysteresis-like behavior and undergoes the first-order phase transition.

2.9. NASICON-type $Na_3M_2(PO_4)_3$, (M = divalent metal) pyrophosphates

NASICON-type $Na_3M_2(PO_4)_3$, (M = Zn, Mn, Cu, Pb, etc.) and various pyrophosphates were proposed as potential candidates for sodium-ion battery cathode [30]. Among the pyrophosphates, $Li_2FeP_2O_7$, $Na_2MnP_2O_7$, $Na_2PbP_2O_7$ and $Na_2ZnP_2O_7$ compounds have been synthesized and investigated [7, 29]. Attempts to improve the properties of material involved various cationic substitutions in the above-mentioned double phosphates, new compounds such as $Na_2Fe_{1-x}Mn_xP_2O_7$, $NaCsMnP_2O_7$, $NaCsMn_{0.35}Cu_{0.65}P_2O_7$, Mn-doped $Na_2ZnP_2O_7$ were synthesized. There were also attempts to improve the battery cathode by adding carbon nano tubes to sodium iron pyrophosphate

$Na_2MnP_2O_7$ is a promising sodium-ion battery cathode material. Electrical properties of $Na_2MnP_2O_7$ ceramics were analysed by impedance spectroscopy in the broad frequency range from 10 Hz to 10 GHz. Temperature dependencies of conductivity indicated a phase transition taking place in the grains of ceramics at 663 K, which was also evidenced by differential thermal analysis and thermal X-ray diffraction. In addition, close to the room temperature protonic conductivity strongly influences the total conductivity of the ceramics. Both newly observed phenomena may be important for overall sodium battery performance.

Although the $Na_2MnP_2O_7$ structure and electrochemical properties were studied, all the investigations on this compound were performed only at the room temperature. Consequently, the studies of high temperature behaviour of $Na_2MnP_2O_7$ powder and ceramics were carried out.

$Na_2MnP_2O_7$ was synthesized by solid state reaction from stoichiometric amounts of $Na_2C_2O_4$, MnC_2O_4 $2H_2O$, and $NH_4H_2PO_4$. The initial compounds were mixed in ethyl alcohol for 3 h. The mixture was heated for 6 h at 300 °C in silicon carbide crucible in Ar/H_2 atmosphere, milled and pelletized (500 kg/cm^2). Then the pellet was heated up to 620 °C (ramp rate of 10 °C/min), annealed for 6 h in a tubular furnace under a steady Ar/H_2 flow, and cooled down to room temperature in Ar/H_2 atmosphere. Finally, the pellet was heated at 700 °C for 6 h, cooled down to room temperature (in Ar/H_2 atmosphere) and milled. Differential thermal analysis and thermogravimetry (SDT Q600) was performed on heating and cooling the powder from room temperature to 620 °C with 10 K/min heating/cooling rate. Thermal X-ray powder diffraction (XRPD) has been performed at 30 °C, 100 °C, 300 °C, 400 °C and 500 °C in air with Cu Kα radiation on a Panalytical Xpert MPD diffractometer equipped with the X' Celerator detector and an Anton Paar HTK 12 furnace. The diagrams were recorded in 2θ range from 7 to 80° with a step of 0.017° and 100 s per step.

The temperature dependence of $Na_2MnP_2O_7$ ceramics total conductivity suggested the phase transition taking place in this compound at 660 K. This phase transition has been approved by DTA and thermal XRPD experiments. To the best of our knowledge, it has never been reported before. Surprisingly, a significant decrease of conductivity was observed on heating ceramics up to 370 K. It was shown that a very small amount of water in the sodium-manganese-pyrophosphates affects their room temperature conductivity, in this case, Na^+ and H^+ must be mixed at the same time. The high proton conductivity at the room temperature and humid ambient atmosphere can have a crucial impact on the performance of the studied material as a sodium battery cathode. The mixed Na+-ionic and proton conductivity in $Na_2MnP_2O_7$, however, could possibly find another application in the future.

2.10. Preparation, structure, surface and impedance spectroscopy of $Na_2Zn_{0.5}Mn_{0.5}P_2O_7$ ceramics

For search new Na-based pyrophosphate materials for application in the secondary sodium ion batteries $Na_2Zn_{0.5}Mn_{0.5}P_2O_7$ powder was synthesized by solid state reaction and ceramics were sintered [31]. The structure studies of the powder were conducted too.

The $Na_2Zn_{0.5}Mn_{0.5}P_2O_7$powder has been synthesized by solid-state reaction method from stoichiometric amounts of Na_2CO_3, ZnO and MnO (all chemically pure). The precursor was mixed and then stoichiometric amount of 85% H_3PO_4 (diluted with distilled water 1:1) was added very slowly, while mixing. The obtained mixture was heated in silica-carbon crucible at 393 K for 5 h and milled. After milling, the obtained powder was pressed into pellets at 50 MPa. The pellets were heated at 673 K for 4 h and subsequently at 923 K for 6 h. The tubular furnace with steady Ar/H_2 flow was used in all heating steps. After the annealing, the pellet was cooled down to RT in Ar/H_2 atmosphere. The obtained product was milled into ceramic powder.

The analysis of XRD patterns show that $Na_2Zn_{0.5}Mn_{0.5}P_2O_7$ powder at RT consists of two phases: $Na_2MnP_2O_7$ crystallizes in triclinic space group $P\bar{1}$ (XRD card 074-2586) and $Na_2ZnP_2O_7$ crystallizes in the tetragonal space group $P4_2/mmm$ (XRD card 01-070-5836) The analysis showed that the obtained composite consists of 38.64 wt.% $Na_2MnP_2O_7$ phase and 61.36 wt. % $Na_2ZnP_2O_7$ phase. The lattice parameters, unit cell volume (*V*), angles (α, β, γ), formula units in the unit cell (Z) and theoretical density (d_t) of both phases at RT are presented in Table 2.8 and Fig. 2.21.

Table 2.8. **Summary of X-ray diffraction analysis of $Na_2Zn_{0.5}Mn_{0.5}P_2O_7$ powder at room temperature**

Phase	*a*, Å	*b*, Å	*c*, Å	α, deg	β, deg	γ, deg	*V*, Å^3	Z	d_t, g/cm^3
$Na_2MnP_2O_7$	9.89(4)	11.08(5)	12.46(3)	148.48	121.98	68.35	595.18(15)	4	3.07
$Na_2ZnP_2O_7$	7.72(5)	10.27(4)	–	–	–	–	612.13(15)	4	3.10

In the temperature interval from 360 K to 700 K, the total electrical conductivity of $Na_2Zn_{0.5}Mn_{0.5}P_2O_7$ increases with temperature according to Arrhenius law, but the activation energy change was found at about 630 K (Fig. 2.21). This change was associated with a phase transition taking place in $Na_2MnP_2O_7$ phase. The temperature hysteresis of the total electrical conductivity value was found at heating and cooling of $Na_2Zn_{0.5}Mn_{0.5}P_2O_7$ ceramics in the temperature from 300 K to 360 K. Non-Arrhenius behaviors of temperature dependence of conductivity can be associated with dehydration of the samples.

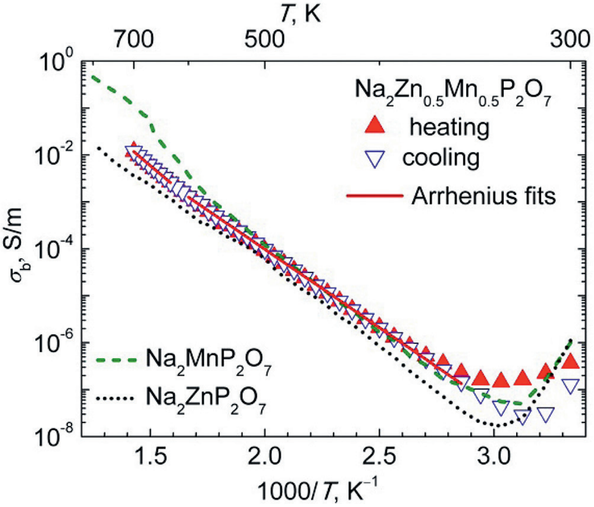

Figure 2.21. **Temperature dependences of bulk electrical conductivity of $Na_2Zn_{0.5}Mn_{0.5}P_2O_7$ ceramics during heating and cooling. Conductivities of $Na_2ZnP_2O_7$ and $Na_2MnP_2O_7$ phases are also presented for comparison**

2.11. Synthesis, structure and impedance spectroscopy of $NaCsZn_{0.5}Mn_{0.5}P_2O_7$ pyro-phosphate ceramics

The evolution of Na^+ ion batteries stimulates the search of new materials for such energy storage devices. In this study, $NaCsZn_{0.5}Mn_{0.5}P_2O_7$ pyrophosphate powder was synthesized by solid state reaction and ceramics were sintered [8].

$NaCsZn_{0.5}Mn_{0.5}P_2O_7$ powders were prepared by a solid-state reaction method from stoichiometric mixture Na_2CO_3, ZnO, MnO, $CsNO_3$ (all precursors were chemically pure) in Ar/H_2 atmosphere. The stoichiometric mixture was mixed and very slowly 85% H_3PO_4 (diluted with distilled water 1:1) was added and mixed. The obtained product in silica crucibles was heated in Ar/H_2 atmosphere at temperature 393 K for 4 h. After milling, the obtained powder was pressed into pellets with pressure of 50 MPa. The pellets were sintered at 673 K temperature for 6 h, and then at 923 K temperature for 4 h. Tubular furnace under a steady Ar/H_2 flow was used for sintering. After annealing the obtained product in Ar/H_2, the atmosphere was cooled down to RT milled again and the obtained powder was heated at 993 K temperature for 4 h.

The results of XRD measurements show that $NaCsZn_{0.5}Mn_{0.5}P_2O_7$ powder prepared by solid state reaction is a mixed phase solid solution. Three different phases were detected in the X-ray diffraction patterns of the powder. $NaCsZnP_2O_7$ (65.61 wt.%), $NaCsMnP_2O_7$ (15.35 wt.%) and $Cs_2MnP_4O_{12}$ (19.04 wt.%) phases were found in the powder at the room temperature. We have not found the information about structure measurements of $NaCsZnP_2O_7$ compound in the literature. The results of XRD patterns' analysis reveal that $NaCsZnP_2O_7$ compound belongs to the monoclinic symmetry (space group $P2_1/n$) with four formula units in the unit cell. The analysis of $NaCsMnP_2O_7$XRD patterns demonstrate that this phase crystallizes in the orthorhombic symmetry (space group $Cmc2_1$) (PDF

01-089-5449). The $Cs_2MnP_4O_{12}$ crystallizes in monoclinic structure (space group $P2_1/n$). The lattice parameters, unit cell volume (V), angle (β), formula units in the unit cell (Z) and theoretical density (d_t) of the three phases at RT are presented in Table 2.9 below.

Table 2.9. **Summary of X-ray diffraction analysis of $NaCsZn_{0.5}Mn_{0.5}P_2O_7$ powder at room temperature**

Phase	Space group	a, Å	b, Å	c, Å	β	V, Å^3	Z	d_t, g/cm^3
$NaCsMnP_2O_7$	$Cmc2_1$	5.3203	15.0477	7.9974		784.37	4	3.534
$NaCsZnP_2O_7$	$P2_1/n$	13.0105	7.6912	7.4241	91.03	742.79	4	3.258
$Cs_2MnP_4O_{12}$	$P2_1/n$	7.9809	13.2416	11.5396	101.98	1192.91	4	3.545

The results of XRD measurements has shown anomalies of the lattice parameters in temperature range (400–500) K in orthorhombic $NaCsMnP_2O_7$ and in temperature range (500–600) K in monoclinic $Cs_2MnP_4O_{12}$, but the symmetry group of above-mentioned compounds has not changed. It is possible that the detected anomalies of electrical properties are caused by disordering in the $NaCsMnP_2O_7$and $Cs_2MnP_4O_{12}$ lattices.

Electrical properties of $NaCsZn_{0.5}Mn_{0.5}P_2O_7$ ceramics were investigated by impedance spectroscopy in the temperature range of 300–700 K, and in the frequency range of 10 Hz – 3 GHz. In the temperature interval 420 K to 700 K, the total electrical conductivity of $NaCsZn_{0.5}Mn_{0.5}P_2O_7$ increases with temperature according to Arrhenius law (Table 2.10). At 480 K and 590 K temperatures, the changes of activation energy of total electrical conductivity were found. In this case also it is possible that the detected anomalies of electrical properties are caused by disordering in the $NaCsMnP_2O_7$ and $Cs_2MnP_4O_{12}$ lattices.

Table 2.10. **Values of total electrical conductivity (σ_{10Hz}) of $NaCsZn_{0.5}Mn_{0.5}P_2O_7$ ceramic at various temperatures (T) and its activation energies at heating ($\Delta E_{tot\text{-}h}$) and cooling ($\Delta E_{tot\text{-}c}$)**

T, K	Heating		Cooling	
	σ_{10Hz}, S/m	$\Delta E_{tot\text{-}h}$, eV	σ_{10Hz}, S/m	$\Delta E_{tot\text{-}c}$, eV
450	$1.19 \cdot 10^{-9}$	0.46	$4.14 \cdot 10^{-10}$	0.50
550	$3.17 \cdot 10^{-8}$	0.86	$1.3 \cdot 10^{-8}$	0.86
650	$8.88 \cdot 10^{-7}$	1.16	$5.42 \cdot 10^{-7}$	1.41

2.12. Conclusions

The following conclusions were obtained from the investigation:

1. X-ray diffraction analysis has shown that a partial substitution of Al^{3+} by Y^{3+} in $Li_{1.3}Al_yY_{x-y}Ti_{1.7}(PO_4)_3$ (x = 0.3; y = 0.1, 0.2), which belongs to NASICON-type compounds, causes an increase in the lattice parameters and theoretical density of

the compound. This variation can be caused by different values of the ionic radii of Al^{3+} by Y^{3+} ions.

2. The results of the investigation of electrical conductivities have shown that the increase of stoichiometric parameter y in $Li_{1.3}Al_yY_{x-y}Ti_{1.7}(PO_4)_3$ (x = 0.3; y = 0, 0.1, 0.15, 0.2, 0.3) system leads to the increase of bulk conductivity (σb) values.
3. The increase of the stoichiometric parameters x, y and amount of impurities $LiTiPO_5$ in the $Li_{1+4x}Ti_{2-x}Nb_yP_{3-y}O_{12}$ (x = 0.1, 0.2, 0.3; y = 0, 0.1, 0.2, 0.3) compounds lead to the decrease of total and bulk conductivities and increase of their activation energies.
4. An increase of lithium content in $Li_{1+4x}Ti_{2-x}(PO_4)_3$ (where x = 0.2, 0.5) compounds leads to the increase of the volume of the lattice, the decrease of the theoretical density of the compounds, and the increase of total and bulk electrical conductivities.
5. The changes of activation energy of σtot (ΔE_{tot}) at 550 K and 528 K temperatures for $LiFeP_2O_7$ and $Li_{0.9}Fe_{0.9}Ti_{0.1}P_2O_7$, respectively, can be related to the structure phase transitions detected by XRD measurements.
6. The anomalies of ΔE_{tot} of $Li_{4x}Ti_{1-x}P_2O_7$ (x = 0.06, 0.1, 0.2) compounds in the temperature range from 520 to 580 K were found. The changes of ΔE_{tot} can be related to some disordering in the supercell.
7. From Mössbauer spectroscopy it is evident that there exist two different ferric iron positions in the $Li_3Fe_{1.2}Sc_{0.75}Y_{0.05}(PO_4)_3$ compound. The hyperfine parameters of iron ions are consistent with the octahedral coordination. Changes in quadrupole splitting at 380 K are in good agreement with observed changes in the conductivity and activation energies. Lowering the temperature, the system shows hysteresis-like behavior and undergoes the first-order phase transition.
8. The temperature dependence of $Na_2MnP_2O_7$ ceramics' total conductivity suggested the phase transition taking place in this compound at 660 K. To the best of our knowledge, it has never been reported before.

   Surprisingly, a significant decrease of conductivity was observed on heating ceramics up to 370 K. A very small amount of water in the sodium-manganese-pyrophosphates affects their room temperature conductivity, in this case, Na^+ and H^+ must be mixed at the same time. The high proton conductivity at the room temperature and humid ambient atmosphere can have a crucial impact on the performance of the studied material as a sodium battery cathode. The mixed Na^+ – ionic and proton conductivity in $Na_2MnP_2O_7$, however, can possibly find another application in the future.
9. The temperature hysteresis of total electrical conductivity value was found at heating and cooling of $Na_2Zn_{0.5}Mn_{0.5}P_2O_7$ ceramics in the temperature from 300 K to 360 K. Non-Arrhenius behaviors of temperature dependence of conductivity can be associated with dehydration of the samples.
10. $NaCsZn_{0.5}Mn_{0.5}P_2O_7$ powder is a mixed-phase solid solution, which consists of $NaCsZnP_2O_7$ (65.61 wt.%), $NaCsMnP_2O_7$ (15.35 wt.%) and $Cs_2MnP_4O_{12}$ (19.04 wt.%) phases. The changes of lattice parameters with temperature were analysed for all three phases by XRD. The anomalies of lattice parameters were observed in the temperature region (400–500) K for $NaCsMnP_2O_7$ and in the temperature range (500–600) K for $Cs_2MnP_4O_{12}$. These anomalies can be caused by structural disordering in these phases. It is possible that the detected anomalies of electrical properties are caused by disordering in the $NaCsMnP_2O_7$ and $Cs_2MnP_4O_{12}$ lattices.

2.13. References

1. Knauth, P. (2009) Inorganic solid Li ion conductors: An overview. *Solid State Ionics*, 180, 911–916.
2. Hagman, L. O., Kierkegaard, P. (1968) The Crystal Structure of $NaM_2^{IV}(PO_4)_3$, Me^{IV} = Ge, Ti, Zr. *Acta Chem. Scand*., 22, 1822–1832.
3. Arbi, K., Rojo, J. M., Sanz, J. (2007) Lithium mobility in titanium based Nasicon $Li_{1+x}Ti_{2-x}Al_x(PO_4)_3$ and $LiTi_{2-x}Zr_x(PO_4)_3$ materials followed by NMR and impedance spectroscopy. *J. Eur. Ceram. Soc*., 27, 4215–4218.
4. Aono, H., Sugimoto, E., Sadaoka, Y., Imanaka, N., Adachi, G.-Y. (1991) Electrical property and sinterability of $LiTi_2(PO_4)_3$ mixed with lithium salt (Li_3PO_4 or Li_3BO_3). *Solid State Ionics*, 47, 257–264.
5. Barpanda, P., Nishimura, S-I., Yamada, A. (2012) High-voltage pyrophosphate cathodes. *Advanced Energy Materials*, 2, 841–859.
6. Shakoor, R. A., Park, C. S., Raja, A. A., Shin, J. and Kahraman, R. (2016) A mixed Iron-manganese based pyrophosphate cathode, $Na_2Fe_{0.5}Mn_{0.5}P_2O_7$, for rechargeable sodium ion batteries. *Phys. Chem. Chem. Phys.,* 18(5), 3929–3935.
7. Daugėla, S., Šalkus, T., Kežionis, A., Venckutė, V., Valdniece, D., Dindune, A., Barre, M., Orliukas, A. F. (2017) Anomalous temperature-dependent electrical properties of $Na_2MnP_2O_7$. *Solid State Ionics*, 302, 72–76.
8. Orliukas, A. F., Venckutė, V., Daugėla, S., Kežionis, A., Dindune, A., Valdniece, D., Ronis, J., Lelis, M., Mosiałek, M., Šalkus, T. (2017) Synthesis, structure and impedance spectroscopy of $NaCsZn_{0.5}Mn_{0.5}P_2O_7$ pyrophosphate ceramics. *Solid State Ionics*, 302, 92–97.
9. Kežionis, A., Butvilas, P., Šalkus, T., et al. (2013) Four-electrode impedance spectrometer for investigation of solid ion conductors. *Rev. Sci. Instrum*., 84, 013902-1-8.
10. Kežionis, A., Kazakevičius, E., Šalkus, T., Orliukas, A. F. (2011) Broadband high frequency impedance spectrometer with working temperatures up to 1200 K. *Solid State Ionics*, 188, 110–113.
11. Šalkus, T., Kazakevicius, E., Reklaitis, J., Venckute, V., Daugela, S., Davidonis, R., Baltrūnas, D., Dindune, A., Valdniece, D., Orliukas, A. F. (2017) Study of the $Li_3Fe_{1.2}Sc_{0.75}Y_{0.05}(PO_4)_3$ ceramics by impedance and Mössbauer spectroscopy. *Solid State Ionics*, 302, 30–34.
12. Venckutė, V., Banytė, J., Kazlauskienė, V., Miškinis, J., Šalkus, T., Kežionis, A., Kazakevičius, E., Dindune, A., Kanepe, Z., Ronis, J., Orliukas, A. F. (2010) Preparation structure and electrical properties of $Li_{1+4x}Ti_{2-x}Nb_yP_{3-y}O_{12}$ (where x = 0.1, 0.2, 0.3., y = 0, 0.1, 0.2, 0.3) ceramics. *Lithuanian J. Phys*., 50. 435–443.
13. Orliukas, A. F., Šalkus, T., Kežionis, A., Dindune, A., Kanepe, Z., Ronis, J., Venckutė, V., Kazlauskienė, V., Miškinis, J., Lukauskas, A. (2012) Structure and broadband impedance spectroscopy of $Li_{1.3}Al_yY_{x-y}Ti_{1.7}(PO_4)_3$ (x = 0.3., y = 0.1, 0.2) solid electrolyte ceramics. *Solid State Ionics*, 225, 620–625.
14. Orliukas, A. F., Venckutė, V., Miškinis, J., et al. (2013) X-ray photoelectron and broadband impedance spectroscopy of $Li_{1+4x}Ti_{2-x}(PO_4)_3$ (where x = 0.2, 0.5) solid electrolyte ceramics. *Lithuanian J. Phys*., 53, 244–254.
15. Venckutė, V., Miškinis, J., Kazlauskienė, V., et al. (2014) XRD, XPS, SEM/EDX and broadband impedance spectroscopy study of pyrophosphate ($LiFeP_2O_7$ and $Li_{0.9}Fe_{0.9}Ti_{0.1}P_2O_7$) ceramics. *Phase Transitions*, 87(5), 438–451.
16. Elbouaanani, L. K., Malaman, B., Gérardin, R. (1999) Structure refinement and magnetic properties of C–$Fe(PO_3)_3$ studied by neutron diffraction and Mössbauer techniques. *Journal of Solid State Chemistry*, 148, 455–463.
17. Dindune, A., Kanepe, Z., Kazakevičius, E., Kežionis, A., Ronis, J., Orliukas, A. F. (2003) Synthesis and electric properties of $Li_{1+x}M_xTi_{2-x}(PO_4)_3$ (where M = Sc, Al, Fe, Y, x = 0.3) superionic ceramics. *Journal of Solid State Electrochemistry*, 7, 113–117.
18. Salkus, T., Kazakevicius, E., Kezionis, A., et al. (2010) XPS and ionic conductivity studies on $Li_{1.3}Al_{0.15}Y_{0.15}Ti_{1.7}(PO_4)_3$. *Ceramics Ionics*, 16, 631–637.

19. Robertson, A., Fletcher, J. G., Skakle, J. M. S., West, A. R. (1994) Synthesis of $LiTiPO_5$ and $LiTiAsO_5$ with the α-Fe_2PO_5 Structure. *Journal of Solid State Chemistry*, 109, 53–59.
20. Venckutė, V., Miškinis, J., Kazlauskienė, V., et al. (2014) XRD, XPS, SEM/EDX and broadband impedance spectroscopy study of pyrophosphate ($LiFeP_2O_7$ and $Li_{0.9}Fe_{0.9}Ti_{0.1}P_2O_7$) ceramics. *Phase Transitions*, 87(5). https://doi.org/10.1080/01411594.2013.857021
21. Sobiestianskas, R., Dindune, A., Kanepe, Z., et al. (2000) Electrical properties of $Li_{1+x}Y_yTi_{2-y}(PO_4)_3$ (where x, y = 0.3, 0.4) ceramics at high frequencies. *Materials Science and Engineering*, B76,184–192.
22. Bogusz, W., Dygas, J. R., Krok, F., et al. (2001) Electrical conductivity dispersion in Co-doped NASICON samples. *Physica Status Solidi (a),* 183, 323–330.
23. Orliukas, A. F., Bohnke, O., Kežionis, A., et al. (2012) Broadband impedance spectroscopy of some Li^+ and $V_0^{\bullet\bullet}$ conducting solid electrolytes. *Advanced Electromagnetics*, 1(1), 70–75.
24. Orliukas, A. F., Šalkus, T., Kežionis, A., et al. (2011) Structure and broadband impedance spectroscopy of $Li_{1.3}Al_yY_{x-y}Ti_{1.7}(PO_4)_3$ (x = 0.3., y = 0.1, 0.2) solid electrolyte ceramics. 18th Int. Conf. Solid State Ionics, Warsaw, July 3–8, Abstracts, 240.
25. Venckutė, V., Dobrovolskis, P., Šalkus, T., et al. (2015) Preparation and Characterization of Solid Electrolytes Based on TiP_2O_7 Pyrophosphate. *Ferroelectrics*, 479(1), 101–109.
26. Orliukas, A. F., Fung, K.-Z., Venckutė, V., et al. (2014) SEM/EDX, XPS and impedance spectroscopy of $LiFePO_4$ and $LiFePO_4$/C ceramics. *Lithuanian J. Physics*, 54(2), 106–113.
27. Šalkus, T., Kazakevicius, E., Reklaitis, J., et al. (2016) Study of the $Li_3Sc_{1.6}\ Fe_{0.4}(PO_4)_3$ and $Li_3Sc_{0.75}\ Y_{0.05}\ Fe_{1.2}(PO_4)_3$ NASICON-type materials by impedance and Mössbauer spectroscopy. 12th Int. Symp. ISSFIT-12, July 3–7, 2016, Kaunas, Lithuania, Abstracts, 110.
28. Bykov, A. B., Chirkin, A. P., Demyanets, L. N., et al. (1990) Superionic conductors $Li_3M_2(PO_4)_3$ (M = Fe, Sc, Cr): Synthesis, structure and electrophysical properties. *Solid State Ionics*, 38, 31–52.
29. Daugėla, S., Šalkus, T., Kežionis, A., et al. (2016) Anomalous temperature-dependent electrical properties of $Na_2MnP_2O_7$. *Solid State Ionics*, 302, 72–76.
30. Palomares, V., Casas-Cabanas, M., Castillo-Martinez, E., Han, M. H., Rojo, T. (2013) Update on Na-based battery materials. A growing research path. *Energy Environ. Sci.,* 6, 2312–2337.
31. Venckutė, V., Dindune, A., Valdniece, D., et al. (2017) Preparation, structure, surface and impedance spectroscopy of $Na_2Zn_{0.5}Mn_{0.5}P_2O_7$ ceramics. *Lith. J. Phys*., 57(3), 183–193.

2.14. Kopsavilkums

Pētīti NASICON-a tipa tīklveida (vai karkasveida) fosfātu materiāli, kā arī fāžu veidošanās likumsakarības multikomponentās neorganisko fosfātu sistēmās, lai sintezētu jaunus savienojumus, noteiktu to struktūru un īpašības un perspektīvā izmantotu jaunu, alternatīvu, ekoloģiski tīru enerģijas avotu cieto elektrolītu (ar ātru jonu pārnesi) ieguvei un izstrādei (gāzu sensoros – vides monitoringā, baterijās – enerģētikā, akumulatoros). Litija jonu vadītājus (cietos elektrolītus) var izmantot arī jauna tipa katodu aizsargslāņa iegūšanā.

Pierādīts, ka NASICON-a tipa savienojumos, piemēram, $LiTi_2^{IV}(PO_4)_3$, Ti^{IV}, aizvietojot ar trīsvērtīgajiem Sc, Al, Y u. c. joniem, var iegūt savienojumus ar ievērojami lielāku elektrovadītspēju (sevišķi istabas temperatūrā vai tuvu tai), jo tiek izmainīti režģa parametri un radīta iespēja palielinātai Li^+ jonu mobilitātiei, t. i., elektrovadītspējai. Tāpēc mūsu darba mērķis ir **jaunu** Li^+ (Na^+) neorganisko fosfora savienojumu sintēze un izpēte, pētot likumsakarības starp kristālu struktūru, elementārsastāvu un jonu vadītspēju šajos materiālos.

Pētījumus sadarbības projektā var iedalīt vairākās grupās.

1. NASICON-a tipa **litija jonu vadītāji** kā cietie elektrolīti litija jonu baterijās.
   Kā zināms, kopējā un tilpuma vadītspēja $LiTi_2(PO_4)_3$ keramikai ir $2.5{\cdot}10^{-6}$ un $6.3{\cdot}10^{-5}$ Scm^1 atbilstoši. Lai palielinātu elektrovadītspēju, tika sintezēti modificēti NASICON-a tipa savienojumi: $Li_{1+4x}Ti_{2\text{-}x}(PO_4)_3$ ($x = 0.2, 0.5$), $Li_{1.3}Al_yY_{x\text{-}y}Ti_{1.7}(PO_4)_3$ ($x = 0.3$, $y = 0.1, 0.2$), $Li_{1+4x}Ti_{2\text{-}x}Nb_yP_{3\text{-}y}O_{12}$ ($x = 0.1, 0.2, 0.3$ un $y = 0, 0.1, 0.2, 0.3$), $Li_3Fe_{1.2}Sc_{0.75}Y_{0.05}(PO_4)_3$.
2. Iegūti arī vairāki katodu materiāli litija jonu baterijām. Jaunie **pirofosfāti** sintezēti cietfāžu reakcijās sistēmās $Li_{1\text{-}x}Fe_{1\text{-}x}Ti_xP_2O_7$ ($x = 0, 0.1$) un $Li_{4x}Ti_{1\text{-}x}P_2O_7$ ($x = 0, 0.06, 0.1, 0.2$), lai izmantotu kā perspektīvus elektrodu materiālus daudzkārtēji uzlādējamās baterijās. Iegūti arī $LiFePO_4$ un $LiFePO_4/C$ katodu materiāli ar olivīna struktūru.
3. Pēdējos gados atklāts, ka litija jonu baterijas sekmīgi aizstāj **Na-metāla pirofosfātu** tipa savienojumi, lai tos izmantotu nātrija jonu bateriju katodu materiāliem. Tāpēc tika sintezēti, pētīti un salīdzināti jauni fosfora savienojumi daudzkomponentu sistēmās $Na_{2\text{-}x}A_xMP_2O_7$ (M = Mn, Zn, A = Cs), lai perspektīvā tos izmantotu sadarbības projekta mērķiem. Cietfāžu reakcijās sintezēti un pētīti šādi savienojumi: $Na_2Zn_{0.5}Mn_{0.5}P_2O_7$, $NaCsZn_{0.5}Mn_{0.5}P_2O_7$, $Na_2MnP_2O_7$.

Izmantojot jaunākās pētniecības metodes, pētījumu rezultāti ļāva secināt, ka daļa iegūto fosfātu materiālu ir perspektīvi praktiskai izmantošanai.

Pētījumiem izmantota rentgendifrakcijas metode (XRD) struktūras parametru noteikšanai, impedances spektroskopija (IS) keramisko paraugu elektrovadītspējas mērīšanai, rentgenstaru fotoelektronu spektroskopija (XPS) vai elektronu spektroskopija (ESCA) ķīmiskai analīzei. Skenējošā elektronu mikroskopija (SEM) vai enerģijas dispersijas rentgenstaru spektroskopija (EDX) lietota kompozītu sastāva noteikšanai, Mesbauera spektrometrija – dzelzs jonu valences pētījumiem sintezētajos paraugos u. c.